Evaneszente Lichtstreuung

Fortgeschrittenenpraktikumsbericht

vorgelegt von
Hermann Böttcher & Jannik Dornseiff

an der

Universität Konstanz

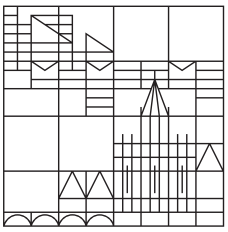

Mathematisch-Naturwissenschaftlichen Sektion
Fachbereich Physik

Tutor: Hugo Wendehenne

Konstanz, 2018

Abstract

Contents

List of Figures

List of Tables

1 Introduction

This experiments serves to examine the position fluctuations of polystyrene particles with a diameter of

$$a = 4{,}28\,\mu\text{m}$$

in an aqueous dispersion that is highly dilute. The observed motion is called the *Brownian motion* (compare section 2.2). To this end, the form of the potential surrounding the single particles is to be determined. Moreover, the determination of the dependency of the diffusion coefficient on the distance between particle and the walls of the cuvette containing the dispersion along with the total distance for a given particle are main goals of the experiment. Regarding the used optical tweezers, the light force on the particles is measured. Last, through measurements of silica particles' movement in aqueous dispersions with different concentrations of salt, the variation of the screening length is examined.

The measurements are done using optical tweezers to trap particles. Furthermore, an evanescent field field is utilized for analysis.

2 Physical background

2.1 Forces on the particles

There are several forces affecting particles suspended in a solution. Most relevant for this experiment are the gravitational, the electrostatic double layer, the Van der Waals and the light force (the latter when using the optical tweezers).

Gravitational force:
The particles interact with the gravitational field of the earth. If their density is higher than the density of the solution that they are suspended in, the particles sink. In front of a wall, where the individual particle is affected by a repulsive force, a potential well forms. The gravitational potential V_{G} can be described as

$$V_{\mathrm{G}} = \frac{4\pi R^3}{3} g(\rho_{\mathrm{p}} - \rho_{\mathrm{m}})z = F_{\mathrm{G}} z, \tag{2.1}$$

with the density of the particle ρ_{p} and of the medium ρ_{m}, the earth acceleration g, the particles radius R and the distance from the wall z.

Eletrostatic double layer force:
The eletrostatic double layer force accounts for the repulsion between particles with the same charge and attraction between those particles of opposite charge. In this experiment, it describes the interaction between particles and the wall. If the particles are suspended in an electrolyte solution, as is the case here, the Poisson equation describes the relation between the electrostatic potential $\Phi(\vec{r})$ and the elementary charge e, $\vec{r}$ being the distance between the two interacting particles. The equation is given by

$$\Delta\Phi(\vec{r}) = -\frac{e^2}{\epsilon k_{\mathrm{B}} T} (\underbrace{\rho_+(\vec{r}) + \rho_-(\vec{r})}_{\rho(\vec{r})},$$

where $\rho_+(\vec{r})$ ist the cation and $\rho_-(\vec{r})$ the anion concentration, ϵ the permittivity, k_{B} the Boltzmann constant and T the temperature.

If the two concentrations are symmetrical, as is the case for monovalent electrolytes like KBr, the Poisson-Boltzmann equation takes the form

$$\Delta\Phi = \frac{\beta e^2}{\epsilon} 2\rho_+ \cdot \sinh\Phi = \underbrace{\frac{e^2}{\epsilon k_{\mathrm{B}} T} \sum_i \rho_i q_i^2}_{=\kappa^2} \cdot \sinh\Phi$$

using the inverse Debye length κ, with q_i as the ion charge and $r \in G$, G being the area which is neither particle nor surface. Introducing the surface charge density of the particles particles σ_{p} and of the wall σ_{w} and z as the distance between particle surface and wall yields

$$\beta V_{dl}(z) = \frac{64\pi\epsilon a}{\beta e^2} \gamma_p \gamma_w e^{-\kappa(z)},$$

$$\gamma_{\mathrm{w/p}} = \tanh\left[\frac{1}{2}\sinh^{-1}\left(\frac{\beta e \sigma_{\mathrm{w/p}}}{2\epsilon\kappa}\right)\right],$$

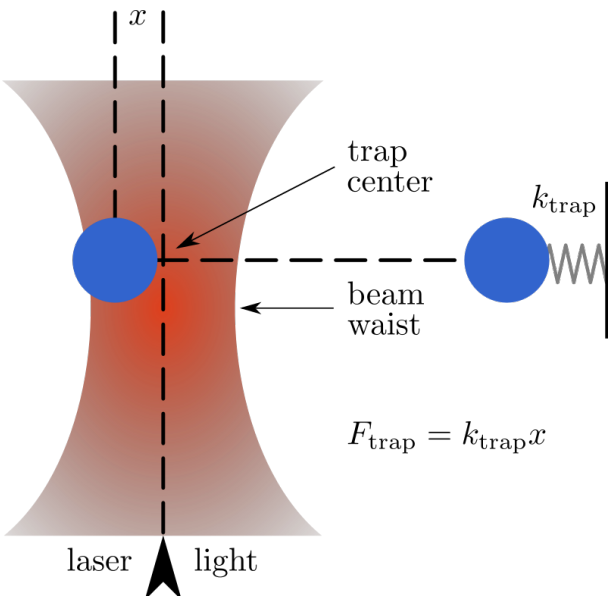

Figure 2.1 Particle trapped by an optical tweezer. The dielectric particle gravitates towards the beam center slightly above the beam waist. [8]

with $\beta = 1/k_{\text{B}}T$ as known from thermodynamics.

Van der Waals force:
In comparison to the previously described electrostatic force, the Van der Waals force is much weaker. Moreover, it occurs mostly as an attractive force in nature. Microscopically, it is derived from the interactions between the fluctuating dipolmoments of the particles. Integration of the particle-particle and the particle-wall Van der Waals force over the sphere wall symmetry of this experiment provides

$$\beta V_{disp}(z) = \frac{A(z)}{6k_B T}\left(\frac{2R}{z}\frac{z+R}{z+2R} - \ln\frac{z+2R}{z}\right), \tag{2.2}$$

with the distance between particle surface and wall z, R the particle radius and $A(z)$ the Hamaker constant.

Light force with optical tweezers:
Counteracting some of the previously mentioned forces, optical tweezers can be used to hold particles in place by utilizing the light force. The light force accounts for the impulses of the icident photons being transferred to the particle when absorbing or reflecting the photons.

To keep it simple, a one dimensional system is regarded. The graviational force acting in negative x-direction $\vec{F}^x_{\text{G}}$ can be counteracted by light force in positive x-direction $\vec{F}^x_{\text{L}}$ to keep a particle floating at $x = x_0 = const.$ yielding

$$\vec{F}^x_{\text{G}} = -\vec{F}^x_{\text{L}}.$$

But optical tweezers can also hold dielectric particles in place against forces perpendicular to the light beam. To this end, a slightly focalised laser beam is utilized which holds the particle in the focus point as illustrated in 2.1.

The force which moves the particle towards the beam's center is called the gradient force. It only moves the particle towards the center, if the refractive index of the particle is larger then the one of the solution in which the particle is suspended, though. If this is the case and there is an intensity gradient, the gradient force moves the particle towards the point of the highest intensity. The procces is similar to a dielectric being sucked into a capacitor. With a strong focus point it is also possible for the gradient force to override the light force if they have opposite directions. For optical tweezers in x- and y-direction the potentials are

$$V_{\nabla,x}(x) = C_x P x^2 \tag{2.3}$$

$$V_{\nabla,y}(y) = C_y P y^2 \tag{2.4}$$

with the laser power P and the parameter C depending on particle size, focus radius, refractive indices and more.
Finally, for the z direction the light force and the gravitational force add up to

$$F^z_{\mathrm{G,eff}} = F^z_{\mathrm{L}} + F^z_{\mathrm{G}}. \tag{2.5}$$

[4]

2.2 Brownian motion

The motion of particles suspended in a fluid resulting from their collision with fast moving molecules (or atoms) of the fluid is called the *Brownian motion*.

Within a fluid in thermal equilibrium at a given temperature, no preferential direction of flow exists. Therefore, the movement of the fluid's molecules is random yielding no linear or angular momenta over time. Sufficiently small particles suspended in this fluid move in random patterns, too, changing their velocities $\vec{v}$ upon colliding with one of the fluid's molecules. As a matter of fact, the observation has been deemed evidence for the existence of individual water (fluid) molecules.

Because of the sheer number of involved fluid molecules, the many-body interactions resulting in the *Brownian motion* cannot be solved relying only on classical mechanics. To put a number to it, the number of collisions of a single particle suspended in the fluid (a so called *Brownian particles*) with the fluid molecules is roughly of the order 10^{14}. Therefore, among others, Albert Einstein produced a probabilistic model using statistical mechanics. Einstein started by formulating a diffusion equation for the *Brownian particle*. To this end, he regarded a one dimensional x-space with the origin at the initial position of the modelled *Brownian particles*. Assuming the conservation of the number of fluid molecules and introducing the density function $\varphi(\Delta)$, with the random variable Δ, he expanded the *Brownian particle* density ρ at a time $t+\tau$ in a Taylor series

$$\begin{aligned}
\rho(x,t) + \tau\frac{\partial\rho(x)}{\partial t} + \cdots = \rho(x,t+\tau) &= \rho(x,t)\cdot\int_{-\infty}^{\infty}\varphi(\Delta)\mathrm{d}\Delta \\
&= \rho(x,t)\cdot\int_{-\infty}^{\infty}\varphi(\Delta)\mathrm{d}\Delta - \frac{\partial\rho}{\partial x}\cdot\int_{-\infty}^{\infty}\Delta\varphi(\Delta)\mathrm{d}\Delta \\
&\quad + \frac{\partial^2\rho}{\partial x^2}\cdot\int_{-\infty}^{\infty}\frac{\Delta^2}{2}\varphi(\Delta)\mathrm{d}\Delta + \cdots \\
&= \rho(x,t)\cdot 1 + 0 + \frac{\partial^2\rho}{\partial x^2}\cdot\int_{-\infty}^{\infty}\frac{\Delta^2}{2}\varphi(\Delta)\mathrm{d}\Delta + \cdots .
\end{aligned}$$

While the integral in the second line equals one by definition of the probability, terms with even partials vanish due to symmetry of the 1D space. The above equation is leads to

$$\begin{aligned}
\frac{\partial\rho}{\partial t} &\approx \frac{\partial^2\rho}{\partial x^2}\cdot\int_{-\infty}^{\infty}\frac{\Delta^2}{2\tau}\varphi(\Delta)\mathrm{d}\Delta \\
&= D\cdot\frac{\partial^2\rho}{\partial x^2}
\end{aligned} \tag{2.6}$$

if only terms of Δ with orders smaller than 2 are regarded and using the *mass diffusivity* or *diffusion coefficient*

$$D = \int_{-\infty}^{\infty}\frac{\Delta^2}{2\tau}\varphi(\Delta)\mathrm{d}\Delta. \tag{2.7}$$

[7]

2.2.1 Brownian motion in proximity of the cavity walls

In section 2.2, only the fluid's molecules surrounding the *Brownian particles* have been taken into account for the diffusion equation eq. (2.6). When the fluid is confined in a cavity though, the

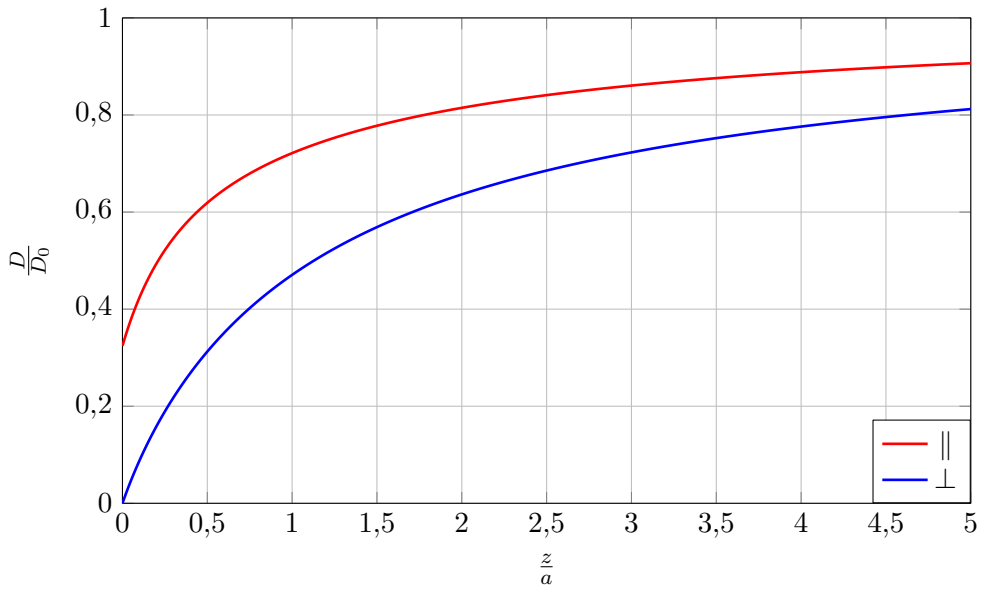

Figure 2.2 Distance dependent diffusion coefficients for a particle of diameter a at a distance z from the walls for parallel and perpendicular components of motion (compare section 2.2.1).

cavity's walls affect the flow of the fluid. This statement can be proven by simply regarding a fluid molecule or *Brownian particle* next the cavity wall. It's motion's component orthogonal to the wall is limited to one direction which is away from the wall. The interaction between the confining walls and the particles is called *hydrodynamic interaction*.

The mathematical description of this phenomenon makes use of distance z dependent diffusion coefficients

$$D_{\parallel}(z) = D_0 \left[1 - \frac{9}{16}\left(\frac{a}{z+a}\right) + \frac{1}{8}\left(\frac{a}{z+a}\right)^3 - \frac{45}{256}\left(\frac{a}{z+a}\right)^4 - \frac{1}{16}\left(\frac{a}{z+a}\right)^5 + \cdots\right] \tag{2.8}$$

$$\begin{aligned} D_{\perp}(z) &= D_0 \left[\frac{4}{3}\sinh(\alpha)\sum_{n=0}^{\infty}\frac{n(n+1)}{(2n-1)(2n+3)}\left(\frac{2\sinh((2n+1)\alpha)+(2n+1)\sinh(2\alpha)}{4\sinh^2((n+\frac{1}{2})\alpha)-(2n+1)^2\sinh^2(\alpha)}-1\right)\right]^{-1} \\ &\approx D_0 \cdot \frac{6\left(\frac{z}{a}\right)^2+2\frac{z}{a}}{6\left(\frac{z}{a}\right)^2+9\frac{z}{a}+2} \end{aligned} \tag{2.9}$$

for the motion orthogonal ($\perp$) and parallel ($\parallel$) to the walls, where z is the distance between particle and wall and $\alpha = \arccos\left(\frac{z+a}{a}\right)$. For the approximation of eq. (2.9) please refer to [2]. The diffusion coefficients are plotted in fig. 2.2. As expected from the thought experiment this section has been introduced with, $D_{\perp}(z=0) = 0$, whereas $D_{\parallel}(z=0) \neq 0$. [4]

2.2.2 Langevin equation

A different approach to the *Brownian motion* of colloidal particles respecting interactions with an interface makes use of the *Langevin equation*. Herefore, the approach through Langevin dynamics yields the equation

$$\Delta\vec{r} = \frac{\vec{D}}{k_{\mathrm{B}}T}\cdot\vec{F}\Delta t + \nabla\cdot\vec{D}\Delta t + \vec{X},$$

where $\vec{D}$ is the direction of motion dependent diffusion coefficient, $k_{\mathrm{B}}T$ the thermal energy, $\vec{F}$ the external force acting on the particle (comapre section 2.1) and $\vec{X}$ is the Brownian contribution to $\Delta\vec{r}$. Moreover, $\vec{r}$ is the particles position and Δt the time interval, which will be restricted later.

The change of the particles position due to external forces $\vec{F}$ is the so called *drift*, which makes the first term on the righthand side the *drift-term*. As the diffusion coefficient depends on the particle's

position in proximity of interfaces, the second term can be identified as the *gradient term*. Finally, the third term describes the contribution of the *Brownian motion*. As during the conducted experiment the measured particles will be trapped by optical tweezers, only the the component perpendicular to the surface of the cuvette needs to be regarded. Therefore, the above equation is written in scalar form

$$\Delta h = \frac{D}{k_\mathrm{B}T} F \Delta t + \frac{\mathrm{d}D}{\mathrm{d}h} \Delta t + \Delta h_\mathrm{Brownian}, \tag{2.10}$$

D and F representing the normal components of the diffusion coefficient and the force vectors (regarding the surface of the cuvette), respectively, Δh being the total change of distance between particle and the cuvette's wall during the time interval Δt.

$$h_\mathrm{Brownian} = \chi \sqrt{2D\Delta t}$$

is therefore change of the distance between particle and interface due to the *Brownian motion* during Δt, where χ is randomly chosen from a set of normally distributed numbers with a mean of zero and standard deviation of one. Using this identity, eq. (2.10) becomes

$$\Delta h = \frac{D}{k_\mathrm{B}T} F \Delta t + \frac{\mathrm{d}D}{\mathrm{d}h} \Delta t + \chi \sqrt{2D\Delta t}.$$

For this equation to be physical, Δt needs to be longer than the relaxation time of the *Brownian fluctuations* and at the same time Sufficiently small as to be able to regard D and F as constant. Using $\Delta t \to 0$ within these bounds, the *Brownian term* is prominent as it only scales with $\sqrt{\Delta t}$, whereas the other two terms scale with Δt. This leads to Δh being normally distributed with the variance

$$\sigma^2_{\Delta h} = 2D\Delta t. \tag{2.11}$$

Regarding the case where $t \to \infty$, the *Brownian motion* as a fluctuation does not change the particles' positions effectively. The potential well trapping the particle $\phi(h)$ becomes prominent. Therefore, the time dependent variance is given by

$$\sigma^2_{\Delta h} = \sigma^2_{\Delta h,\infty} \left[1 - \exp\left(-\frac{2D\Delta t}{\sigma_{\Delta h,\infty}} \right) \right],$$

$\sigma_{\Delta h,\infty}$ being the variance at large times. This is in accordance with eq. (2.11) when Taylor expanding around $\Delta t = 0$. As the variance should reach zero for $\Delta t \to \infty$, the probability of a particle with initial position h_0 to being found at $h_0 + \Delta h$ is concluded to be

$$p(h_0 + \Delta h) = A \exp\left(\frac{-\phi(h_0 + \Delta h)}{k_\mathrm{B}T} \right).$$

Here, A is a normalization constant and $\phi(h_0 + \Delta h)$ the potential energy of the particle at position $h_0 + \Delta h$. For the form of the potential, the forces mentioned in section 2.1 must be respected. [6]

2.3 Evanescent field

To analyze the position fluctuations of the particles in the aqueous dispersion, an evanescent field is utilized. An evanescent field is a field of any kind, were there is no net energy flow in any given direction. In this experiment, this is achieved by total reflection.
If a lightbeam hits a transition between two media with the refraction indices n_1 for medium 1 and n_2 for medium 2 at the angle Θ_1, part of it is refracted at the angle Θ_2 and part of it is reflected at the angle Θ_1. This relation is described by Snell's law

$$n_1 \sin(\Theta_1) = n_2 \sin(\Theta_2).$$

If $n_1 > n_2$, there is a critical angle Θ_c at which all the light is reflected and non of it transmits into medium 2 with

$$\Theta_c = \arcsin\left(\frac{n_2}{n_1}\right).$$

Still, an exponentially decaying field component of the incident wave enters the second medium. As it decays exponentially, there is no energy flow and it is therefore an evanescent wave. The resulting field distribution in medium 2 is given by

$$E_r = E_0 \exp\left(-\frac{\beta}{2}z\right) \exp\left(i\frac{n_1}{n_2}\sin(\Theta_1)kx - i\omega t\right),$$

$2/\beta$ being the characteristic decay length. This means that the wave decays with β^{-1} in the medium and this decay is defined as

$$\beta^{-1} = \frac{\lambda_0}{4\pi\sqrt{n_1^2 \sin^2\Theta_1 - n_2^2}},$$

which shows that the penetration depth diverges at the critical angle ($\Theta_1 = \Theta_c$) and the minimum penetration depth is

$$\beta^{-1} = \frac{\lambda_0}{4\pi\sqrt{n_1^2 - n_2^2}}.$$

[4]

2.4 Determination of the potential form

The following explanations are taken from [3].

The scattering intensity $I(z)$ depends, in the following manner, on the distance z between the particle and the wall:

$$\begin{aligned} I(z) = I_0 \exp(-\beta z) \leftrightarrow z &= -\beta^{-1} \ln\left(\frac{I_z}{I_0}\right) \\ &= -\beta^{-1} \ln I(z) + \underbrace{\beta^{-1} \ln I_0}_{=z_0} \end{aligned} \tag{2.12}$$

Where β^{-1} is the penetration depth of the evanescent field and I_0 is the scatter intensity that results when particles and wall are in direct contact. Without knowing this constant, only relative distances can be determined, since z_0 can not be computed. The absolute distance is determined hydrodynamically in the second section of the evaluation; here $I_0 = 10$ is assumed arbitraily. The Boltzmann equation combines the distance-dependent probability distribution $p(z)$ with the interaction potential $V(z)$ between particle and wall:

$$p(z) = p_0 \exp\left(-\frac{V(z)}{k_\mathrm{B}T}\right) \leftrightarrow \frac{V(z)}{k_\mathrm{B}T} = -\ln\left(\frac{p(z)}{p_0}\right)$$

The distance-dependant probability distribution is calculated using eq. (2.12), and can then be converted into en intensity probability distribiution $N(I)$:

$$p(z) = N(I)\frac{\mathrm{d}I}{\mathrm{d}z} = -\beta N(I) I(z),$$

where $N(I)$ is obtained directly from the measured data as a histogram. The resulting potential is then

$$\frac{V(z)}{k_\mathrm{B}T} = -\ln\left(\frac{-\beta N(I) I(z)}{p_0}\right) = -\ln\left[N(I)I(z)\right] + \ln\left(-\frac{p_0}{\beta}\right). \tag{2.13}$$

Before creating the histogram, the background must first be subtracted from the measured data. This corresponds to the scatter signal in the absence of the particle. For this purpose, the particle can be pulled out of the field of view with the optical tweezers and the background at the measuring position can be determined directly (approximately 10 s to 30 s measurement averaged). The number of bins in the histogram determines the number of potential values that are calculated. The error on the calculated potential value decreases with increasing number of counts per bin. Approximately 100 bins represent a good compromise between a small error of the individual potential values on the one hand and good local resolution on the other. Equation (2.13) potential already has the correct shape, but not yet the correct absolute distance from the surface.

2.5 Hydrodynamic evaluation

This section is taken from [3], too.

For the determination of the potential shape, only the probability distribution has so far been used. However, much more information is available in the measurement data. An analysis of the dynamics of the measured data provides information on the distance dependence of the diffusion coefficient and also allows the determination of the absolute distance. The 3D diffusion coefficient (far from the surface), D_0 is described by the Stokes-Einstein equation

$$D_0 = \frac{k_\mathrm{B} T}{6\pi\eta R},$$

where η is the vescosity of the liquid and R corresponds to the particule's radius. In the vincinity of a wall, where the liquid molecules can not move (stick boundary conditions), the diffusion coefficient becomes distance-dependent and anisotropic (compare section 2.2.1). The distance-dependent diffusion coefficient for diffusion perpendicular to the wall $D_\perp$ was calculated analytically by Brenner as an infinite series [1]. This series can be approximated very well for small distances $z < R$ to

$$D_\perp = \frac{D_0}{\frac{R}{z} + 0,2 \ln\left(\frac{R}{z}\right) + 0,9712}. \tag{2.14}$$

Considering the solution of the Langevin equation for a spherical particle near a wall, the distance-dependent diffusion coefficient can also be determined from the measured trajectory of the particle [5]. To do this, the following procedure is applied:

1. The measured intensity data are converted into distances, whereby an arbitrary value is initially assumed for the scatter intensity at the contact of particle and wall (I_0 in eq. (2.12)). The maximum input voltage of the A/D card of 10 V is for example a realistic starting value for I_0.
2. For the analysis of the dynamics, the measured trajectory is divided into about 20 intervals a_j . For each a_j , a histogram of the distance changes Δz_i is generated within a certain time interval Δt. That under the condition that the i-th distance value z_i measured in the trajectory is in the interval a_j, $z_i = z_{i+k} - z_i$ is calculated and entered into the histogram. The time interval $t = k\delta t_\mathrm{mess}$ is necessarily an integer multiple of the measurement interval δt_mess and $k = 1, 2$, in order not to average over too long time intervals. Neglecting the effects of the interaction potential (curvature), a Gaussian distribution of p the distance changes is to be expected, whose width is $\sigma_{z_i,\Delta t} = \sqrt{2 D_{z_i} \Delta t}$. In principle, $D_{(z_i)}$ can already be determined from the fit parameter $\sigma_{(z_i,t)}$ for a certain Δt. However, a smaller measurement error is obtained if $\sigma_{(z_i,t)}$ against Δt, and $D_{(z_i)}$ is determined from the slope [5].
3. The unknown parameter I_0 is now adapted such that the distance-dependent diffusion coefficient D_z coincide with the theoretical predictions from eq. (2.14) (η and a are known). From this follows the correct absolute particle wall distance for the potential.

In the practice of the experiment, the described evaluation is implemented by a predetermined MatLab routine, in which only I_0 has to be adapted as a parameter.

3 The Experiment

3.1 Experimental setup and conduction

The experimental setup focuses on a glass cuvette holding an aqueous dispersion with colloidal particles. Figure 3.1 shows the relevant part of the experimental setup. Through a prism, a red laser beam is focused on the sample at such an angle, that the beam is totally reflected and only an evanescent light field reaches the colloidal particles. This light is scattered and it's intensity measured at a fixed angle. Simultaneously, a green laser beam is used as an optical tweezer to hold the single particle in place which the red laser is focused on. Depending on the power of the green laser, the particle is trapped in a trap of varying strength.

Using the optical tweezers, a single colloidal particle is trapped. It can be tracked using the footage of a camera. Once the particle is centered on the computer screen by moving the sample holder in a plane not affecting the angles of the incident laser beams, a different objective is rotated in front of the camera, resulting in a stronger amplification. Again, the particle is centered on the computer screen. Then, the intensity of the scattered light is recorded by a computer program over the duration of 20 min. Here, it is important to check from time to time, that the particle has not escaped from the optical tweezers.

This process is repeated for different input voltages of the optical tweezers' green laser: $U_{\text{tweezers}} = 0{,}76\,\text{V}, 0{,}70\,\text{V}, 0{,}65\,\text{V}, 0{,}60\,\text{V}, 0{,}00\,\text{V}$. To measure the spectrum with the optical tweezers turned off, a particle is focused on analogously to the process with the optical tweezers turned on. During the measurement, the position of the sample holder must continuously be readjusted to track the particle.

Then, a spectrum at $U_{\text{tweezers}} = 0{,}75\,\text{V}$ is recorded at a larger incident angle of the red laser (in respect to the normal of the prism's surface and the beam (compare fig. 3.1)). Finally, a dark spectrum of the background noise is taken with the red laser turned off.

3.2 Data analysis

The I_0 values are determined by a trial and error method. We plotted:

$$I(z) = I_0 \exp\left(-\beta z\right)$$

for different I_0 values and compared it to our measured I(z) date as seen in **??**.

The I_0 value were both plots are the closest to each other is chosen. With this set of diagrams we determined the I_0 value for the $U_{\text{tweezers}} = 0{,}75\,\text{V}$ data-set. This was the best looking data-set for I_0 determination,but to not cause any confusion, the measurements conducted for $U_{\text{tweezers}} = 0{,}75\,\text{V}$ did not yield any usable results. There are a lot of *nan* values in the data set, which could therefore not be processed as the other sets. This might be due to the particle being lost from time to time. It is not really clear, as the particle has been observed most of the time of the measurement.

In the following, the step by step evaluation is written down for a new exemplary measurement data set, but I_0 is determined by the same process. To this end, the measurement with the optical tweezers voltage $U = 0{,}70\,\text{V}$ is analyzed in detail. The other measurements are analyzed analogously and therefore,only the results will be presented for each step.

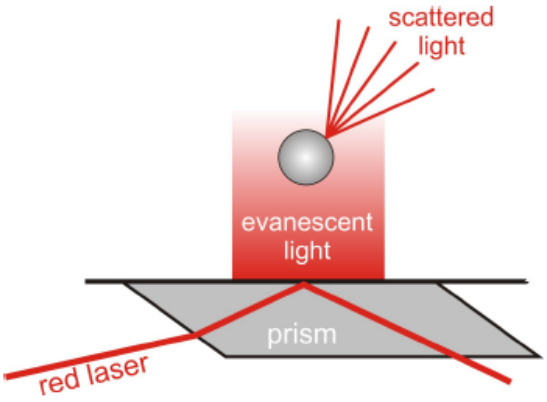

Figure 3.1 Relevant part of the experimental setup. The light of the evanescent field is scattered by the colloidal particles. For more explanations, please refer to section 3.1.

Figure 3.2(a) shows the recorded raw data: The intensity of the scattered light $I(z)$ over a time axis. As the measurement of the background noise yielded a constant zero signal, the correction is irrelevant. z is the distance between the colloidal particle at the wall of the cuvette. The dependency of I on z is given by

$$I(z) = I_0 \exp(-\beta z) \tag{3.1}$$

$$\Rightarrow \quad z = -\beta^{-1} \ln\left(\frac{I(z)}{I_0}\right) = -\beta^{-1} \ln I(z) + \beta^{-1} \ln I_0, \tag{3.2}$$

where β^{-1} is the penetration depth of the evanescent field and I_0 the scatter intensity that results when particles and wall are in direct contact. At this point, only relative distances can be computed as I_0 is an unknown constant. As this constant will be computed in the course of this evaluation, the graph shown in fig. 3.2(b) uses the absolute distance data with the parameter $I_0^{70} = 2,6$. With eq. (2.13) in combination with the determined $I_0^{70} = 2,6$ the potential can be calculated.

The computed potential $V(z)$ of the measurements is illustrated in fig. 3.4 Using the potential's minimum as a breakpoint, it can be divided into two overlaying potentials: An exponential potential for the sharp drop at the beginning, and a linear rising after the minimum signifying the gravitational and the light force. The so divided sections of the potential are fitted with an exponential and a linear curve:

$$\begin{aligned} V_{\text{exp}}(z) &= a \cdot \exp(-bz) + c \\ V_{\text{lin}}(z) &= mz + d. \end{aligned} \tag{3.3}$$

A small data modification needs to be done yet: The potential data is derived from a histogram that sorts by intervals of the Boltzmann distribution. Therefore, the potential data points at high distance values contain only few scattered photons and can therefore be neglected. All in all, the selection of the interval to be fitted with a linear fit is more or less an approximation o the authors to reach the wanted results. These results are plotted in fig. 3.4 along with the potential itself.

At this point, the data of $I_{\text{tweezers}} = 0\,\text{V}$ is used, to determine the gravitational potential. Because in the respective potential, there is no light force to be had since the laser has been turned off during the experiment, the linear part manifests only due to the gravitational potential. Taking the gradient of this potential, which is simply the slope of the fit in this case, the gravitation force on the particle is derived to be

$$F_{\text{gravitational}}^{\text{experimental}} \approx 3{,}9 \times 10^{-13}\,\text{N} \approx 4{,}0 \times 10^{-13}\,\text{N} = \frac{4}{3}\pi r_{\text{particle}}^3 = \rho_{\text{Polysterene}} * g = F_{\text{gravitational}}^{\text{theoretical}},$$

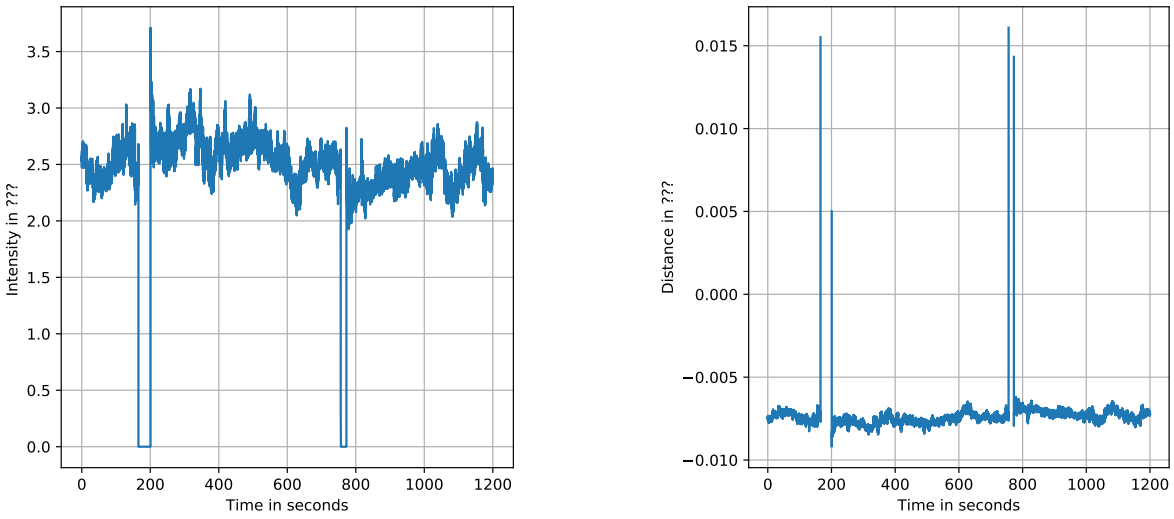

(a) (b)

Figure 3.2 Plots of the recorded raw data with the optical tweezers voltage $U_{\text{tweezers}} = 0{,}70\,\text{V}$. (a) Recorded raw data: Intensity of the scattered light over time. (a) Same data with a processed intensity axis, now showing the distance z between particle and cuvettes walls ($I_0^{70} = 2, 6$).

where $g = 9{,}81\,\frac{\text{m}}{\text{s}^2}$ is the gravitational acceleration on earth's surface, $r_{\text{particle}} = \frac{a}{2} = 2{,}14 \times 10^{-6}\,\text{m}$ the particle's radius and $\rho_{\text{Polysterene}}$ the mass density of polysterene. Since the fit intervall has been optimized to hit close to the theoretical value, there is no way of approximating the uncertainties. The fit parameter error is only a very small secondary error. What could be done for a more precise evaluation is to weigh the different data points using the values of the histogram used to derive the potential form or even using the Boltzmann distribution as a weight.

The light force of the other measurements is now determined by subtracting the linear fit of $I_{\text{tweezers}} = 0\,\text{V}$ from the other linear fits, in explanation

$$V_{\text{Light-Force}} = V_{\text{lin}} - V_{\text{Gravitational}}, \tag{3.4}$$

with the light force potential $V_{\text{Light-Force}}$, the total linear potential V_{lin} and the gravitational potential $V_{\text{gravitational}}$. The results for all measurements are plotted in fig. 3.5(a). Since increasing the voltage of the optical tweezers linearly scales with the number of emitted photons (the wavelength is constant), a linear scaling between light force and the tweezers' voltage is expected. The before mentioned figure shows exactly that, the light forces being

$$\begin{aligned} F_{\text{Light-Force}}(U_{\text{tweezers}} = 0{,}70\,\text{V}) &= -1{,}6 \times 10^{-13}\,\text{N} \\ F_{\text{Light-Force}}(U_{\text{tweezers}} = 0{,}65\,\text{V}) &= -1{,}0 \times 10^{-13}\,\text{N} \\ F_{\text{Light-Force}}(U_{\text{tweezers}} = 0{,}60\,\text{V}) &= -0{,}5 \times 10^{-13}\,\text{N}. \end{aligned}$$

As a result, expectations are that the linear part of the potentials becomes steeper for higher voltages of U_{tweezers}. Figure 3.5(b) shows the comparison of all the measured potentials. As a matter of fact, the expectations are not satisfied by that comparison. The potentials' forms are seem to be disturbed too much to yield a clear tendency. Maybe bigger steps of U_{tweezers} would yield a more suggestive image.

Finally, fig. 3.6 shows the influence of the penetration depth of the evanescent field. Both measurements have been conducted at approximately the same tweezers voltage $U_{\text{tweezers}} = 0{,}76\,\text{V} \approx 0{,}75\,\text{V}$. The penetration depth has been varied by changing the incident angle of the red laser onto the prism. The only significant difference between the two potentials is the shift to higher distances for the smaller penetration depth.

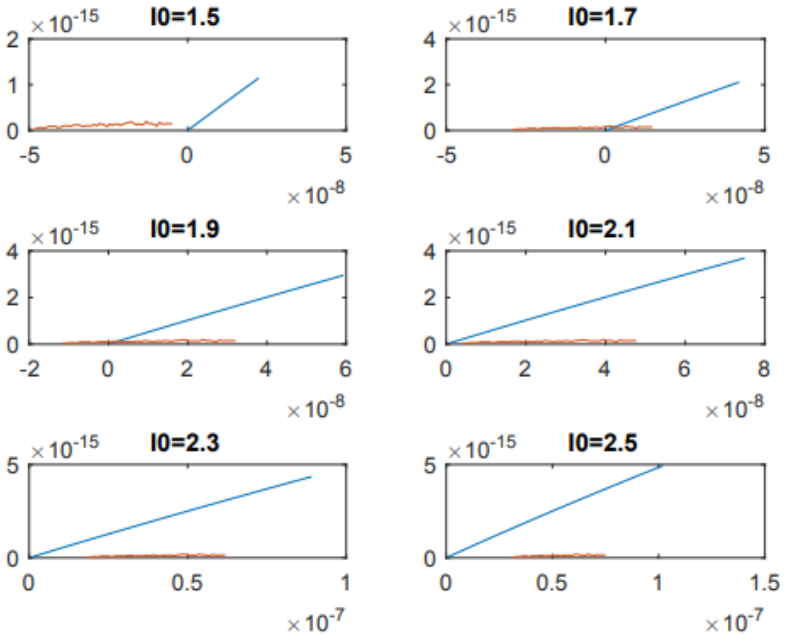

Figure 3.3 Plotted and measured intensity curves layered to find the best fit for I_0. The red line is the measured data, the blue line is the plot and $I_0 = 1,9$ was chosen as the best fit.

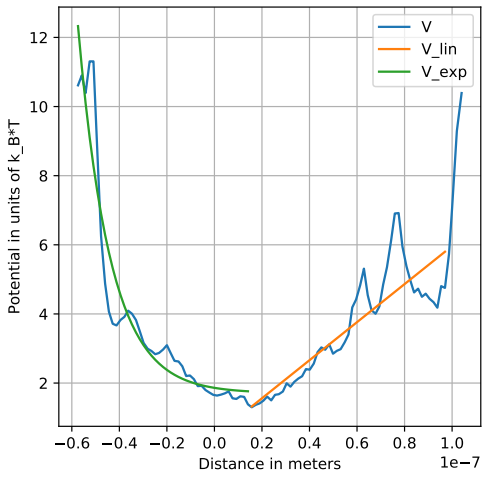

Figure 3.4 Potential computed for the tweezers voltage $U_{\text{tweezers}} = 0{,}70\,\text{V}$. The potential is divided in two overlaying sub-potentials and the respecting fits (compare eq. (3.3)) plotted on top of the potential.

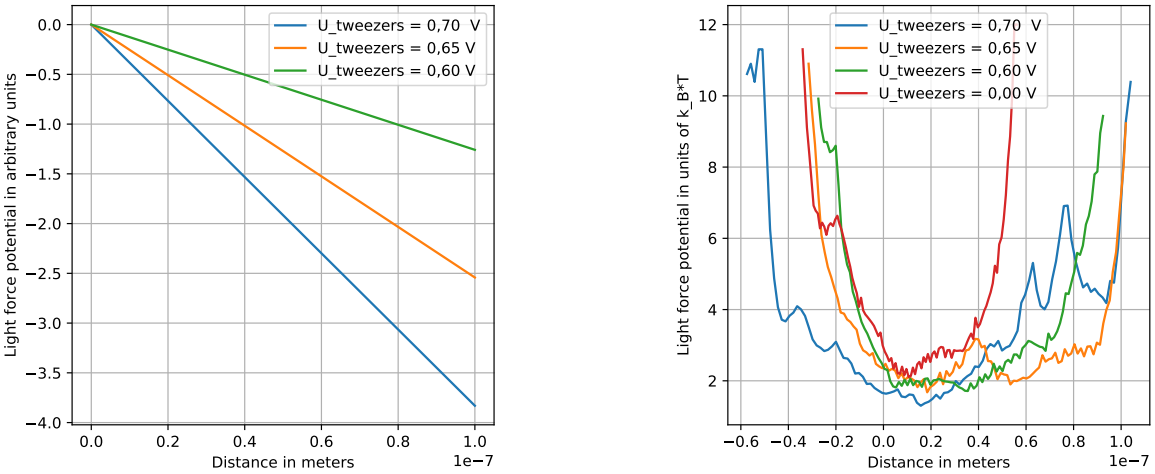

Figure 3.5 (a) Computed light forces (compare eq. (3.4)) for the different voltages U_{tweezers} of the optical tweezers. (b) Comparison of all the measured potentials.

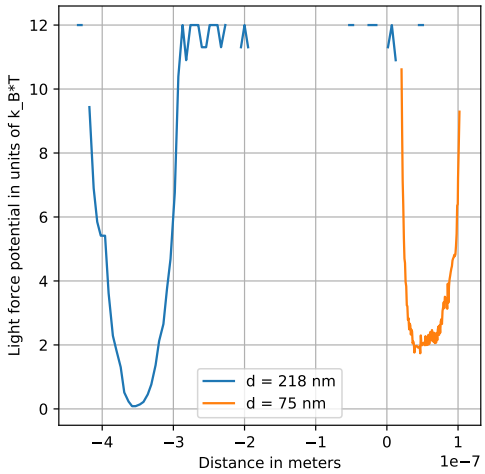

Figure 3.6 Comparison of the potentials derived from two measurements when varying the penetration depth of the evanescent field.

Bibliography

[1] H. Brenner. "The slow motion of a sphere through a viscous fluid towards a plane surface.," in: *Chem. Eng. Sci. 16* 3-4 (1961).

[2] M. A. Bevan und D. C. Prieve. "Hindered diffusion of colloidal particles verry near to a wall: revisited". In: *J. Chem. Phys.* 113 (2000).

[3] R. Bausinger H. Wendehenne. *Evanescent lightfield*. University internal. Nov. 2018.

[4] Laurent Helden. "Untersuchung von Partikel-Wand-Wechselwirkungen mit evaneszenter Lichtstreuung". PhD thesis. University of Constance, May 2003.

[5] R. J. Oetama and J. Y. Walz. "A new approach for analyzing parti- cle motion near an interface using total internal reflection microscopy". In: *J. Colloid Interface Sci.* 284.1 (2005), pp. 323–331.

[6] John Y. Walz Ratna J. Oetama. "A new approach for analyzing particle motion near an interface using total internal reflection microscopy". In: *Colloid and Interface Science* 284 (2005), pp. 323–331.

[7] Wikipedia contributors. *Brownian motion — Wikipedia, The Free Encyclopedia*. [Online; accessed 13-December-2018]. 2018. URL: `https://en.wikipedia.org/w/index.php?title=Brownian_motion&oldid=872665253`.

[8] Wikipedia contributors. *Optical tweezers — Wikipedia, The Free Encyclopedia*. [Online; accessed 11-December-2018]. 2018. URL: `https://en.wikipedia.org/w/index.php?title=Optical_tweezers&oldid=872666703`.